International Journal of Pharmaceutics 417 (2011) 196–203

Contents lists available at ScienceDirect

International Journal of Pharmaceutics

journal homepage: www.elsevier.com/locate/ijpharm

# Benchtop-MRI for *in vivo* imaging using a macromolecular contrast agent based on hydroxyethyl starch (HES)

Ahmed Besheer[a,b,*], Henrike Caysa[a,c], Hendrik Metz[a], Thomas Mueller[c], Jörg Kressler[b], Karsten Mäder[a,**]

[a] Department of Pharmaceutical Technology and Biopharmacy, Institute of Pharmacy, Martin-Luther University Halle-Wittenberg, Wolfgang-Langenbeck-Str. 4, D-06120 Halle/Saale, Germany
[b] Department of Physical Chemistry, Institute of Chemistry, Martin Luther University Halle-Wittenberg, D-06099 Halle/Saale, Germany
[c] Department of Internal Medicine IV, Oncology/Hematology, Medical Faculty, Martin-Luther-University Halle-Wittenberg, D-06120 Halle/Saale, Germany

ARTICLE INFO

*Article history:*
Received 20 September 2010
Received in revised form 17 October 2010
Accepted 19 October 2010
Available online 5 November 2010

*Keywords:*
Hydroxyethyl starch (HES)
Macromolecular contrast agents
Benchtop MRI
Asymmetric flow field flow fractionation (AF4)
Tumor-rim enhancement

ABSTRACT

Magnetic resonance imaging (MRI) is a powerful non-invasive diagnostic tool in the clinical setting. However, the wide spread use of small animal MRI instruments for preclinical research purposes has been limited by the need for strong magnets operating in the range of 4.7–11.7 T. To obtain such strong and homogenous magnetic fields, superconducting electromagnets cooled with liquid helium are used, which highly increases the costs for research studies. Here we report on the use of a pilot 0.5 T benchtop MRI (BT-MRI) operating with a permanent magnet and designed for *in vivo* imaging of mice. It was used to evaluate a novel macromolecular MRI contrast agent based on a Gd-chelate of hydroxyethyl starch (Gd-HES). Images obtained by the BT-MRI showed the high contrast enhancement of Gd-HES, its longevity in the circulation, as well as its utility for tumor diagnosis, urography and angiography. These results demonstrate the potential of the new BT-MRI as a useful research tool, as well as that of Gd-HES as a new MRI contrast agent.



## 1. Introduction

Since its first implementation by Lauterbur (1973) magnetic resonance imaging (MRI) has become a powerful non-invasive diagnostic tool in the clinical setting. MRI is gaining even more importance through the introduction of functional MRI (fMRI) for neuroimaging (Logothetis, 2008), dynamic MRI for blood flow (Varallyay et al., 2009), and other novel applications (Gallagher et al., 2008; Galiana et al., 2008). MRI depends on the phenomenon of nuclear magnetic resonance (NMR), whereby atomic nuclei exposed to a strong magnetic field absorb electromagnetic waves at a characteristic frequency, which falls in the radio frequency range. Using special 3D-encoding techniques, MRI gives a spatial distribution of the density (and relaxation) of protons (Kuperman, 2000).

Despite its high ability to differentiate between internal organs, contrast agents may be required for tissue specific enhancement of the MRI images, particularly soft tissues such as the liver, GIT, cardiovascular system, lymphatic system and the lung. MRI contrast agents that decrease the longitudinal relaxation time (T1) and transverse relaxation time (T2) by roughly the same degree generate a positive contrast in T1-weighed images. These positive contrast agents are usually paramagnetic complexes of $Gd^{3+}$ or $Mn^{2+}$ ions (Caravan et al., 1999; Barrett et al., 2006; Geraldes and Laurent, 2009). By contrast, super paramagnetic iron oxide nanoparticles (SPIONs) lead to a pronounced decrease in T2 compared to T1, and usually give dark spots (negative contrast) in T2-weighed images (Caravan et al., 1999; Barrett et al., 2006; Geraldes and Laurent, 2009).

The commercially available positive MRI contrast agents (CAs), such as Gd-DTPA, Gd-DOTA or Gd-BOPTA have low molar masses. This causes several drawbacks which can be overcome by conjugation to a polymeric carrier. The latter offer the following advantages: (1) reducing the toxicity of metal ions, (2) persistence in the blood, (3) better contrast enhancement, (4) the possibility to attach and deliver other ligands, including therapeutic and targeting moieties, and finally (5) they can be conjugated to a homing device to be targeted to specific tissues (Mulder et al., 2006; Kim et al., 2007). The macromolecular contrast agents are retained in

* Corresponding author at: Department of Pharmacy, Pharmaceutical Technology and Biopharmaceutics, Ludwig Maximilian University, D-81377 Munich, Germany. Tel.: +49 89 2180 77025; fax: +49 89 2180 77020.
** Corresponding author. Tel.: +49 345 55 25167; fax: +49 345 55 27029.
*E-mail addresses:* ahmed.besheer@cup.uni-muenchen.de (A. Besheer), maeder@pharmazie.uni-halle.de (K. Mäder).
*URL:* http://pharmtech.pharmazie.uni-halle.de (K. Mäder).

0378-5173/$ – see front matter © 2010 Elsevier B.V. All rights reserved.
doi:10.1016/j.ijpharm.2010.10.051

the blood, and thus they can act as blood pool contrast agents. This can be used to assess tissue perfusion, blood volume, capillary permeability and vascular anatomy (Schwickert et al., 1995), as well as detecting pathological conditions with enhanced vascular permeability, such as inflammation, myocardial infarction, atherosclerosis, breakdown of the blood–brain barrier and solid tumors (Mulder et al., 2006).

Some macromolecular MRI CAs have been reported, including the conjugates of Gd-DTPA to albumin (Ogan et al., 1987), dextran (Loubeyre et al., 1996; Kroft et al., 1999) and polyamidoamine (PAMAM) dendrimers (Kobayashi and Brechbiel, 2005). However, these examples have problems of immunogenicity, non-biodegradability, or insufficient confinement to the blood pool. Since a biodegradable, non-immunogenic polymer would be the ideal carrier, we modified hydroxyethyl starch (HES) to act as a macromolecular MRI CA. HES is a water soluble, biodegradable polymer widely used as a plasma volume expander (Besheer et al., 2007). Due its favorable properties, it was used for the synthesis of amphiphilic polymers (Besheer et al., 2007), surface modification of nanoparticles (Besheer et al., 2009b), and conjugation to proteins as an alternative to PEGylation (Besheer et al., 2009a). In this study, HES is coupled to DTPA via biodegradable ester bonds and then chelated to Gd. The HES conjugate was characterized using $^1$H NMR, conductometric titration, asymmetric-flow field flow fractionation (AF4) as well as relaxivity measurement, and finally, the contrast enhancement was evaluated in animal models, in comparison to low molar mass Gd chelates using MRI.

Clinical MRI instruments operate in the range of 1.5–3 T, while the more sensitive small animal instruments operate in the range of 4.7–11.7 T. Both types of instruments use expensive, liquid-helium-cooled superconducting electromagnets to obtain such strong and homogenous magnetic fields. Due to the high costs, only few institutions possess dedicated small animal MR scanners. The more available, less sensitive clinical instruments represent an accessible alternative, where the difference in quality could be overcome by longer acquisition times (Beuf et al., 2006; Brockmann et al., 2007). Recently, 0.5 T Benchtop MRI (BT-MRI) instruments have been described for *in vitro* measurements (Metz and Mäder, 2008). The pilot in vivo imaging instrument used in this study has a pore size of 23 mm, and is thus designed for measurements on mice. The BT-MRI uses a permanent magnet, which decreases the costs to a large extent, while providing good quality images. It is the aim of the current study to test (i) if BT-MRI is a feasible approach to get meaningful *in vivo* images in mice with good signal-to-noise ratio, and (ii) to explore the potential of Gd-HES as a new MRI contrast agent.

## 2. Materials and methods

### 2.1. Materials

HES70 ($M_W$ 70,000 g/mol) was a kind gift from Serumwerk Bernburg, Germany, diethylenetriaminepentaacetic acid (DTPA), N,N′-dicyclohexylcarbodiimide (DCC), N-hydroxysuccinimide (NHS), and $GdCl_3{\cdot}6H_2O$ were purchased from Sigma–Aldrich, N,N-dimethylaminopyridine (DMAP) was purchased from Merck, Darmstadt, Germany. Gd-BOPTA (Multihance®, gadopenate dimeglumine) was from Bracco, Milan, Italy.

### 2.2. Methods

#### 2.2.1. Synthesis of the Gd-HES chelates

1.6 g (4 mmol) or 2.4 g (6 mmol) of DTPA was dissolved in 10 ml dry DMF by heating and sonication. After addition of DMAP and heating, DTPA dissolved completely. DCC and NHS were dissolved in 5 ml DMF then added to the DTPA solution. The molar ratio of DTPA:DMAP:DCC:NHS was 4:1:2:2. 1.5 g HES70 (8.1 mmol of anhydroglucose unit – AGU) were dried at 105 °C for 2 h, then dissolved in 10 ml DMF. HES solution was added to the DTPA solution and left to react overnight at room temperature under stirring. The reaction mixture was filtered using a Buchner flask, dialysed for 4 days (MWCO 6–8 kDa), then lyophilized.

For chelation of Gd, 500 mg of the HES-DTPA conjugate were dissolved in 5 ml distilled water (DW). 400 mg $GdCl_3{\cdot}6H_2O$ were dissolved in 5 ml DW and added to the modified HES solution. The mixture was stirred for 1 h, then dialysed against DW for 3 days and lyophilized.

#### 2.2.2. $^1$H NMR spectroscopy

For $^1$H NMR measurements, 50 mg polymer samples were dissolved in 600 μl $D_2O$ alone, or with the addition of 10 mg NaOH, and measured at 400 MHz (Gemini 2000, Varian Inc., USA).

#### 2.2.3. Conductometric analysis

A solution of $GdCl_3{\cdot}6H_2O$ was prepared (120 mg/100 ml DW). Solutions of HES-DTPA in 30 ml DW were prepared. Gd solution was added in steps of 0.5 ml and the conductivity was measured. Measurements were carried out 3 times for each of the modified HES.

#### 2.2.4. Asymmetric flow field flow fractionation (AF4)

Samples were prepared with a concentration of 5 mg/ml in DW preserved with 0.02% w/v sodium azide. For AF4 measurements, the Eclipse FFF system (Wyatt Technology Corp., CA, USA) was used. It was coupled to an 18 angle DAWN EOS MALS detector (Wyatt Technology Corp., CA, USA) and an RI detector Shodex 101 (Shoko America, CO, USA). Samples were filtered through a 0.2 μm filter and 100 μl of the solution were injected into a channel having a 350 μm spacer and a 5 kDa regenerated cellulose ultrafiltration membrane (Nadir C010F, Microdyn-Nadir GmbH). A channel flow of 1 ml/min was maintained, while a linearly decreasing cross flow from 2 ml/min to 0 ml/min over 30 min was used for separation. Data were evaluated using ASTRA software v.4.90.08 (Wyatt Technology Corp., CA, USA).

For HES70, a dn/dc value equal to 0.146 was obtained from the literature (Kulicke et al., 1991). For the other samples, dn/dc was determined by measuring 3 different concentrations, each repeated three times. After correction for the moisture content measured by TGA (approximately 8%, w/w), dn/dc was found to be 0.136 for the Gd chelates of HES-DTPA.

#### 2.2.5. Determination of relaxivity

Samples were dissolved in PBS pH 7.4 (EP) and measured at 37 °C in a 0.5 T benchtop MRI spectrometer (Oxford Instruments, UK). For T1 measurement, the inversion recovery pulse sequence was used, while for T2 measurements, the CPMG sequence was used.

#### 2.2.6. In vivo imaging

*Animals*: 3 male nude mice (NMRI-Foxn1nu, Harlan Winkelmann, Germany) were used. Their age was approximately 80 d when they were injected subcutaneously with 2 different human colon carcinoma cell lines, namely; HT29 on the left side of the abdomen, and DLD-1 to the right side. In each case, 5 million cells suspended in 100 μl PBS were injected. The imaging experiment was conducted 4 weeks after tumor cell injection. For angiography, 3 Balb/c mice (2 males and 1 female) weighing between 15 and 25 g were used.

*Sample preparation*: HES70-DTPA18-Gd (see footnote of Table 1 for sample nomenclature) was dissolved in sterile saline solution to a concentration of 8%, w/v (concentration of Gd is 5 mmol/l). Samples were sterilized by filtration through 0.2 μm filter under

**Table 1**
Molar substitution (MS) of the different HES-DTPA conjugates and the amount of Gd complexed per 1 g as determined from $^1$H NMR and conductometric titration.

| | MS of DTPA (mol%) | Amount of Gd complexed per 1 g HES-DTPA from $^1$HNMR (mmol) | Amount of Gd complexed per 1 g HES DTPA from conductometric titration (mmol) (±S.D. in %) |
|---|---|---|---|
| HES70 DTPA18[a] | 18 | 0.716 | 0.736 (±0.123%) |
| HES70 DTPA25[a] | 25 | 0.884 | 0.876 (±0.53%) |

[a] Sample nomenclature: the number after HES represents the molar mass of the unmodified HES, the number after DTPA represents the MS.

**Fig. 1.** The left photograph shows the Benchtop MRI spectrometer for *in vivo* imaging, while the right one shows an anaesthetized nude mouse with anaesthesia mask (black arrow) and subcutaneously-injected tumors (white arrows).

aseptic conditions. Multihance® was aseptically diluted 1:100 with sterile saline solution to give a concentration of 5 mmol/l before use.

*Administration*: Animals were anaesthetized with a continuous stream of isofluran (Forene®, Abbott) in $O_2$ (2 vol.%, 2 l/min) using an Isofuran Vet. Med. Vaporizer (Drägerwerk AG, Lübeck, Germany). Through the tail vein, each animal was injected 150 μl of Multihance® or 150 μl of HES70-DTPA18-Gd. The injected dose was approximately 0.03 mmol Gd/kg.

*MR imaging*: Imaging was carried out using a prototype benchtop MRI spectrometer for *in vivo* animal studies (Oxford Instruments, UK) (Fig. 1), where transaxial images of each anaesthetized mouse were collected using the following parameters: image sequence: T2 spin echo sequence (T2SS), TR 172 ms, TE 9.8 ms, slice width 3 mm, slice separation 3.5 mm, number of slices 5, averages 16, total time 360 s, field of view 40 mm, and images are 512 × 512 pixels. A 50 μl capillary containing a standard solution of Multihance® was used as a reference (conc. 10 mmol/l).

*Image analysis*: Greyscale images were analyzed using the image analysis freeware JMicroVision v1.2.5. For the renal sinus and cortex, the average of 36 pixels (6 × 6) was used. The same was applied to the tumor center, while for the tumor rim the average of 4 positions (36 pixels for each) was used (see Fig. 2). To be able to compare the measurements, the signal intensity (SI) at the different regions of interest (ROI) was divided by the SI for the reference capillary, and then normalized by dividing it by the signal intensity at time = 0 min.

## 3. Results and discussion

### 3.1. $^1$H NMR and conductometric titration

For the coupling of DTPA to HES, the esterification using DCC/NHS/DMAP was used as mentioned earlier (Besheer et al., 2007). Due to the fact that DTPA is multifunctional, there is a chance for crosslinking. The use of an excess amount of DTPA in relation to DCC/NHS may reduce the degree of crosslinking. Scheme 1 shows the esterification reaction.

$^1$H NMR was used to determine the degree of esterification of HES with DTPA, as seen in Fig. 3. When samples were dissolved in $D_2O$, it was not possible to assign the peaks for the coupled DTPA, probably due to intra- or intermolecular micellization, since DTPA is insoluble in water at neutral pH. Only the peaks from the protons bound to C1 of the AGU could be unequivocally assigned (peak a), together with an additional peak e. The latter is due to the methylene group of the esterified primary alcohols of the polymer backbone. Upon addition of 0.1 N NaOH, a shift of the peaks of the protons bound to C1 was observed, an effect already reported for solutions of NaOH with polysaccharides (Isogai, 1997). More importantly, the peaks for the hydrolysed DTPA can be easily identified, and the peak of the esterified primary alcohols disappears, indicating the hydrolysis of the ester bonds by NaOH. These spectra were used to determine the molar substitu-

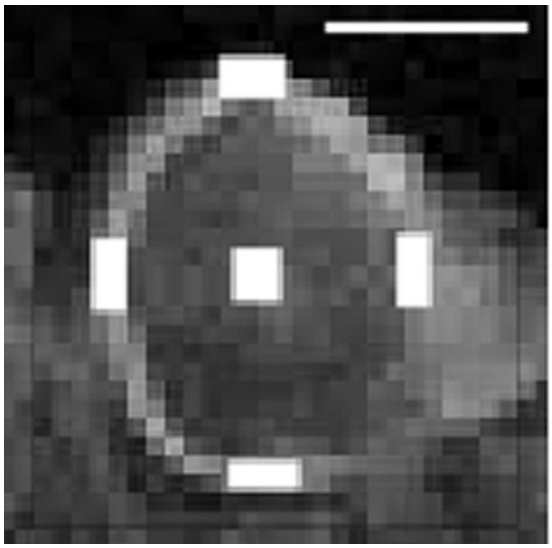

**Fig. 2.** A greyscale image of the tumor area, showing the 4 positions of the tumor rim (white bars) and the tumor center (scale bar equals 0.5 cm).

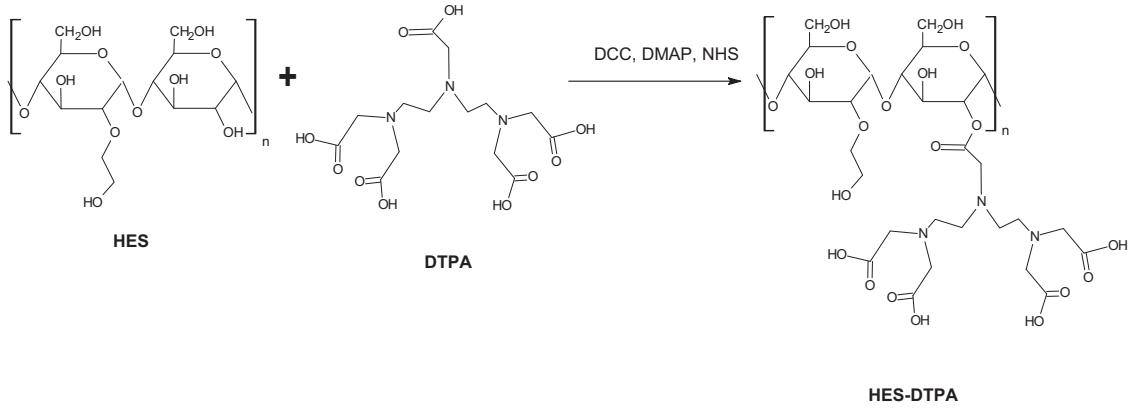


**Scheme 1.** Synthesis of HES-DTPA.

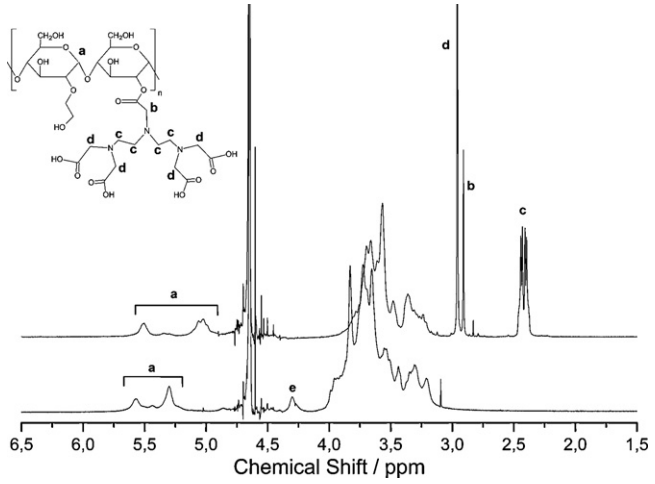


**Fig. 3.** $^1$H NMR spectrum of HES70-DTPA18 dissolved in $D_2O$ (bottom) and in 0.1 N NaOH solution in $D_2O$ (top), together with peak assignment.

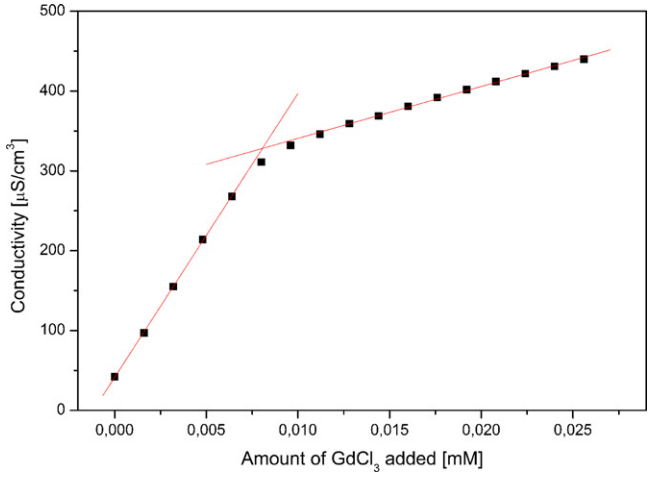


**Fig. 4.** Titration of 11.2 mg HES70-DTPA18 with $GdCl_3$ solution.

tion (number of DTPA molecules attached per 100 AGU) as seen in Table 1.

Another method was used for the determination of the amount of coupled DTPA, namely conductometric titration. The sharp initial increase in the curve for conductometric titration seen in Fig. 4 is due to the release of $H^+$ ions from the DTPA molecule after complexation of $Gd^{3+}$. When all the DTPA molecules are saturated by complexing $Gd^{3+}$ ions, the addition of excess $GdCl_3$ leads to an increase in conductivity, however with a clearly lower slope. This can be explained by the large difference in molar conductivity ($\lambda$) between the protons and the Gd ions, where it amounts to 349.65, and $201.9 \times 10^{-4}$ m$^2$ Smol$^{-1}$, respectively (Lide, 2004). Accordingly, the 4 released protons after complexation contribute to the observed large increase in conductivity. It was possible to calculate the amount of Gd complexed per gram of the macromolecule using $^1$H NMR and the conductometric titration as seen in Table 1, where the results show a very good agreement between the 2 methods.

### 3.2. Asymmetric flow field flow fractionation (AF4)

AF4 has been used for the fractionation and molar mass determination of different natural and semi-synthetic polysaccharides, such as native starches (Roger et al., 2001), glycogen (Rolland-Sabate et al., 2007), chitosan (Augsten and Mäder, 2008), and chemically-modified starches (Wittgren et al., 2002). Such molecules usually have large molar masses and wide molar mass distribution. When compared to high performance size exclusion chromatography (HPSEC), the latter has a lower exclusion limit and cannot resolve molecules of extremely large molar masses (Rolland-Sabate et al., 2007). On the other hand, AF4 can resolve molecules in the range from 5 to $10 \times 10^3$ g/mol (which is equal to few nm for most molecules) upto 50 µm (Rolland-Sabate et al., 2007).

The number average ($M_n$) and weight average ($M_w$) molar masses as well as the polydispersity (PDI) and recovery are given in Table 2. $M_w$ of Gd-HES is clearly higher than that of the original HES, as well as the expected molar mass based on $^1$H NMR results.

**Table 2**
Molar masses, polydispersity and recovery as determined by AF4 coupled to MALS for the unmodified HES sample, as well as the Gd-HES chelates. The estimated molar mass based on the $^1$H NMR results is included for comparison.

| | $M_n$ (kg/mol) | $M_w$ (kg/mol) | Polydispersity ($M_w/M_n$) | Recovery (%, w/w) | Estimated *MW* based on $^1$H NMR results (kg/mol) |
|---|---|---|---|---|---|
| HES70 | 35.8 ± 0.8 | 69.7 ± 2.2 | 1.95 ± 0.02 | 86.1 ± 1.1 | – |
| HES70-DTPA18-Gd | 87.6 ± 4.7 | 205.8 ± 6.1 | 2.38 ± 0.03 | 79.9 ± 0.08 | 107.4 |
| HES70-DTPA24-Gd | 98.7 ± 1.9 | 309.7 ± 32.7 | 3.11 ± 0.29 | 79.1 ± 0.04 | 121.9 |

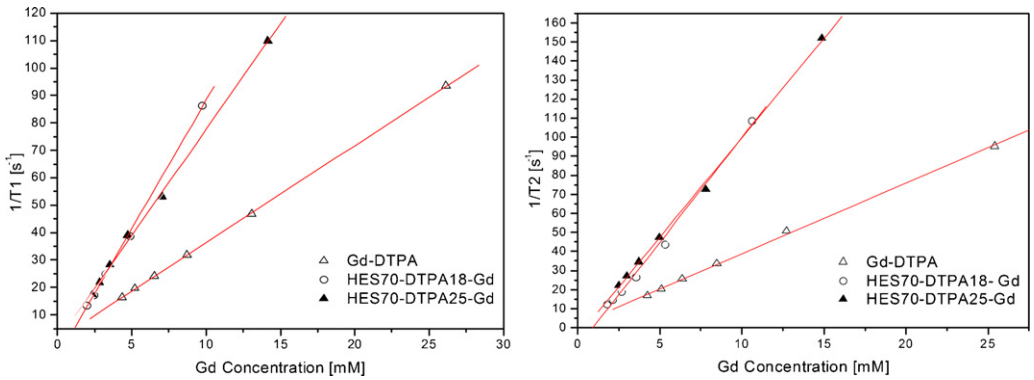


**Fig. 5.** Effect of the concentration of Gd-HES as well as Gd-DTPA on the longitudinal relaxation rate 1/T1 (left) and the transverse relaxation rate 1/T2 (right).

(see Table 2). The increase in the molar mass is probably due to crosslinking. Rebizak et al. (1997) reported a considerable increase in the molar mass after the reaction of aminated carboxymethyl dextran with DTPA. They used different methods for the activation of DTPA, including the synthesis of DTPA bisanhydride, the succinimidyl ester of DTPA, and the mixed anhydride. They observed that, whatever the activation method used, an increase in the molar mass beyond the theoretically expected level occurred. They attributed this to the polyfunctionalization of DTPA and subsequent crosslinking.

### 3.3. Relaxivity

Signal intensity in MRI depends, in addition to the proton concentration and the imaging sequence, on the local longitudinal relaxation rate 1/T1 and transverse relaxation rate 1/T2. The longitudinal and transverse relaxivities, $r_1$ and $r_2$, are defined as the increase in 1/T1 and 1/T2, respectively, as a function of the concentration of the paramagnetic agent (Caravan et al., 1999; Caravan, 2006). Relaxivity can thus be used for the comparison of the efficiency of different contrast agents regarding their signal enhancement in MRI.

Results for relaxivity measurements are shown in Fig. 5 and Table 3. The values of $r_1$ and $r_2$ for Gd-DTPA (3.53 and 3.99 $mM^{-1}\,s^{-1}$, respectively) are close to those reported earlier (Caravan et al., 1999). When compared to the Gd-HES conjugates, the latter show an increase in relaxivity of 2–2.5 times. This increase has been observed for other macromolecular contrast agents, such as the Gd chelates of dextran-DTPA (Armitage et al., 1990), and could be attributed to a decrease of the rotational correlation time due to conjugation to a macromolecule (Armitage et al., 1990).

### 3.4. In vivo imaging

Gd chelates are often used as MRI contrast agents for the detection of solid tumors in man, where the tumor rim usually enhances more strongly than the core (Mitchell et al., 1994; Buadu et al., 1997; Ma et al., 1997; Geirnaerdt et al., 1998; Mussurakis et al., 1998; Kuhl, 2000; Tsien et al., 2005). Using dynamic MRI (i.e. a series of time-dependent images taken rapidly after injection), a low molar mass Gd chelate shows an initial rim enhancement, followed by a washout effect (Morris, 2002). The initial rim enhancement is because of the active peripheral angiogenesis, and thus the high vasculature, while the washout is due to the extravasation of the low-molar-mass CA. The rim enhancement is so characteristic of solid tumors, that it is used for the differentiation between malignant and benign masses (Ma et al., 1997). However, with low molar mass contrast agents, the rapid washout effect necessitates that the images are obtained within the first 2 min after injection (Morris, 2002). Macromolecular MRI CAs have a long circulation time and are confined to the blood pool, giving a longer time window for imaging and pathology-revealing images (Daldrup et al., 1998).

**Table 3**
Longitudinal relaxivity ($r_1$) and transverse relaxivity ($r_2$) for Gd-DTPA and the Gd-HES samples, measured in phosphate buffer pH 7.4 at 37 °C and 20 MHz.

| | Longitidunal relaxivity $r_1$ ($mM^{-1}\,s^{-1}$) | Transverse relaxivity $r_2$ ($mM^{-1}\,s^{-1}$) |
|---|---|---|
| Gd-DTPA | 3.53 | 3.99 |
| HES 70-DTPA 18 | 9.4 | 11 |
| HES 70- DTPA 25 | 7.74 | 10.43 |

Panel a in Fig. 6 shows the T1-weighed, transaxial images of the mouse abdomen before and after administration of Gd-HES. The images show the two xenografted colon carcinomas (right: DLD-1, left: HT29). After i.v. injection of Gd-HES, a clear and persistent rim enhancement can be observed in both tumors for more than 3 h. Moreover, a central accumulation of the contrast agent in the tumor can be seen, which increases with time. In case of the model low molar mass CA, Multihance®, no significant tumor-rim enhancement could be seen in Fig. 6b and d, due to the rapid extravasation and elimination of small CAs (Morris, 2002).

The use of Gd-HES for urography is also tested. Fig. 7a and c shows the kidneys in the T1-weighed, transaxial images for the mouse abdomen. Before injection of the Gd-HES, images obtained by the BT-MRI display a dark renal sinus and a brighter renal cortex. The former usually contains urine, which, being a liquid, has a long T1 and thus appears dark. After injection of Gd-HES, an inversion of the contrast can be seen, where the renal sinus looks brighter than the cortex. The signal enhancement of the renal sinus is 4–5 times that before Gd-HES injection and extends over more than 4 h. After 8 h, the enhancement of the renal sinus returns back close to the state before injection. In contrast, the increase in signal enhancement for the cortex is much lower (Fig. 7c). These results point to the long circulation time of Gd-HES, as well as to its elimination through the kidneys. They also show that an application of Gd-HES to image the urinary tract seems quite feasible. In contrast, the signal enhancement of the low molar mass CA is much lesser and is over a shorter time period.

Fig. 8 shows the results of using Gd-HES for angiography as compared to the Multihance®. While the Gd-HES contrast agent produced a strong contrast allowing the visualization of the blood vessels in the neck area, namely the carotid artery and jugular vein, the low-molar-mass CA did not. Moreover, Gd-HES clearly circulated in the blood for an extended period of time, and could be detected in the circulation even after more than 2.5 h from injection.

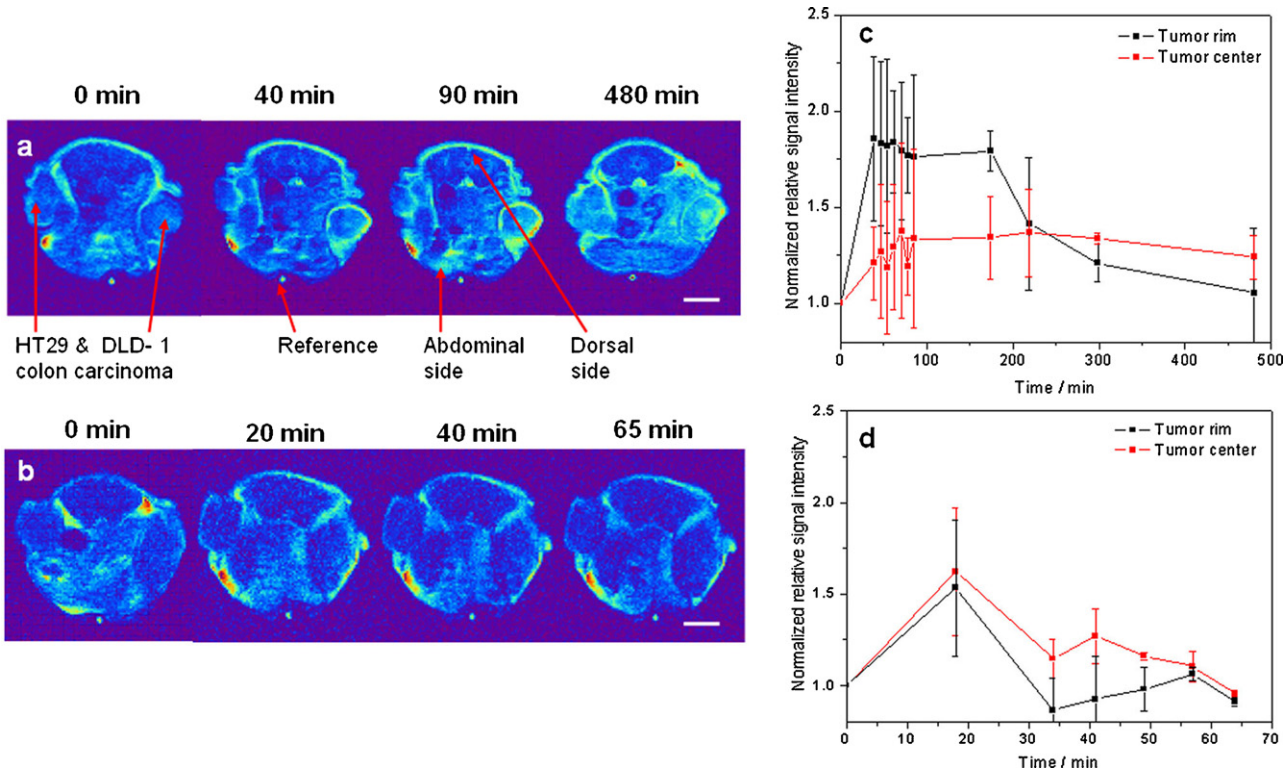


**Fig. 6.** Imaging of tumor-rim enhancement using BT-MRI and Gd-HES: Axial MRI sections (3 mm thick) in nude mice 30 days after s.c. injection of 2 human colon carcinoma cell lines; HT29 (left) and DLD-1 (right). Images are before and after injection of (a) 150 μl of HES 70-DTPA 18-Gd solution (polymer conc. 8%, w/v, ca. 0.03 mmol Gd/kg), or (b) 150 μl of 5 mMol/l Multihance® (0.03 mmol Gd/kg). Scale bar equals 0.5 cm. The graphs to the right show the normalized relative signal intensity in the rim and center of the HT29 tumor after (c) Gd-HES injection, or (d) Multihance® injection.

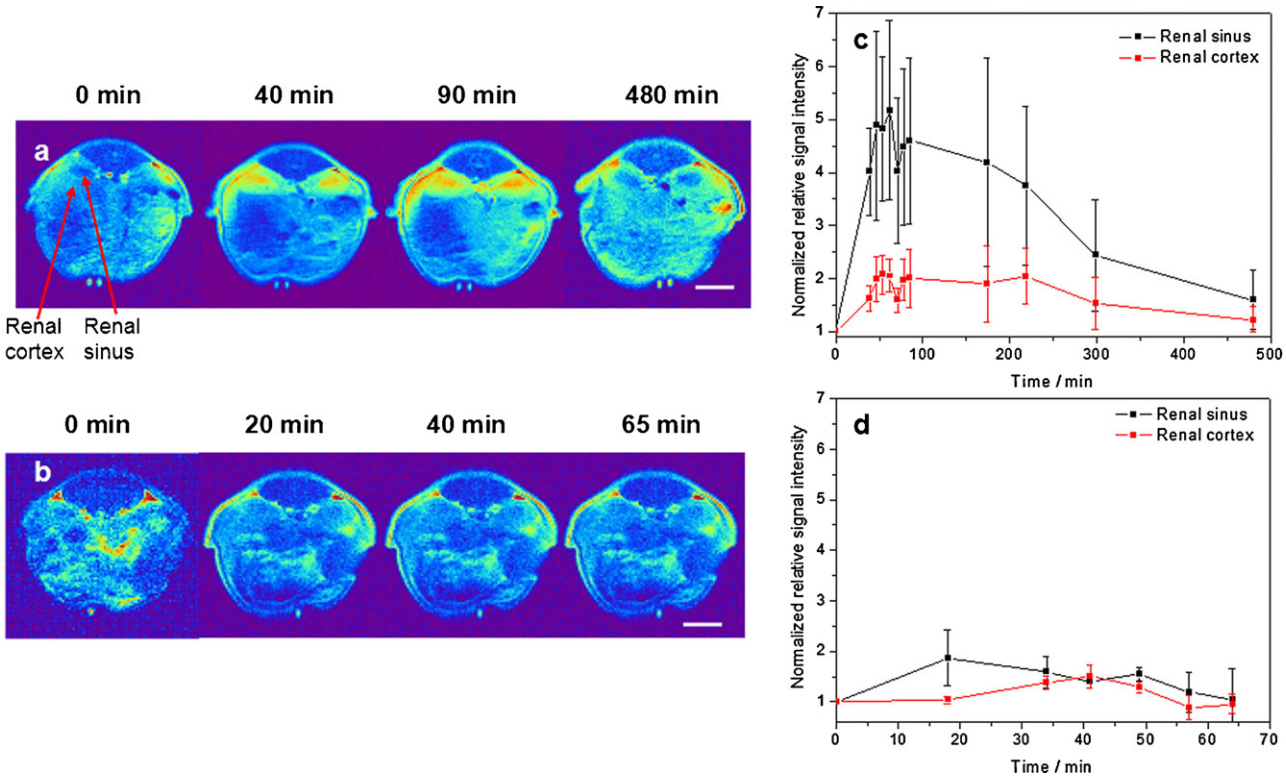


**Fig. 7.** Urography using BT-MRI and Gd-HES: Axial MRI sections (3 mm thick) in nude mice showing the kidneys before and after injection of (a) 150 μl of HES 70-DTPA 18-Gd solution (polymer conc. 8%, w/v, ca. 0.03 mmol Gd/kg), or (b) 150 μl of 5 mMol/l Multihance® (0.03 mmol Gd/kg). Scale bar equals 0.5 cm. The graphs to the right show the normalized relative signal intensity in the renal sinus and cortex after (c) Gd-HES injection, or (d) Multihance® injection.

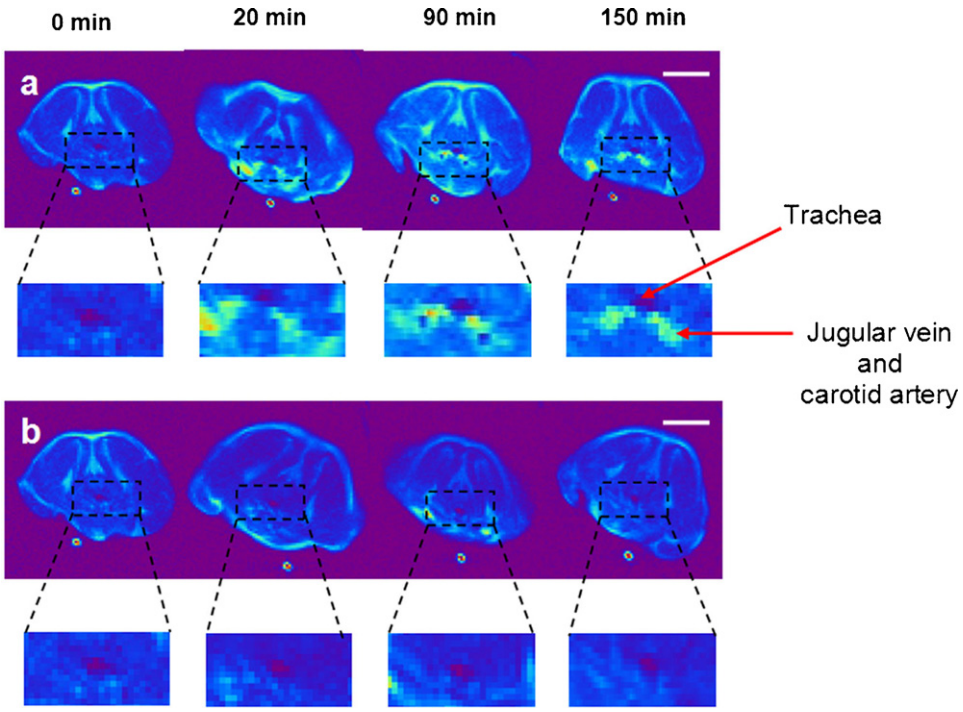


**Fig. 8.** Angiography using BT-MRI and Gd-HES: MRI images of the neck region of Balb/c mice after injection of HES 70-DTPA 18-Gd (panel a) or Multihance® (panel b). The magnified insert shows the trachea, the jugular vein and the carotid arteries. Scale bar equals 0.5 cm.

## 4. Conclusions

HES, having a molar mass of 70,000 g/mol, was esterified with DTPA using DCC, DTPA and NHS. From $^1$H NMR and conductometric titration, the molar substitution of DTPA was found to be between 18 and 24 mol%. The average molar mass and polydispersity of the Gd-HES chelates were analyzed using AF4 coupled to MALS. Results show that the molar mass and polydispersity of Gd-HES increased significantly compared to the original HES. This is attributed to crosslinking due to the inevitable polyactivation of the multifunctional DTPA. Relaxivity of the macromolecular Gd chelate was 2–2.5 times that of Gd-DTPA, pointing out to a better efficiency in signal enhancement. *In vivo* experiments performed on a new pilot BT-MRI instrument concentrated on applying Gd-HES for tumor imaging, as well as urography and angiography. Gd-HES outperformed a model low molar mass CA, showing strong enhancement, higher longevity in the blood and anatomically-revealing images. In general, these results show that the *in vivo* BT-MRI gives images with good signal to noise ratio at low field, qualifying it to perform as a new imaging tool for preclinical studies on mice, and point to the utility of Gd-HES as a novel biodegradable macromolecular contrast agent with possible applications in the clinical setting.

## Acknowledgements

A.B. is thankful for “Exzellenzcluster Nanostrukturierte Materialien, Sachsen-Anhalt” for financial support. Dr. Judith Kuntsche’s support with AF4 measurements is highly appreciated.

## References

Armitage, F.E., Richardson, D.E., Lis, K.C.P., 1990. Polymeric contrast agents for magnetic resonance imaging: Synthesis and characterization of gadolinium diethylenetriaminepentaacetic acid conjugated to polysaccharides. Bioconj. Chem. 1, 374–395.

Augsten, C., Mäder, K., 2008. Characterizing molar mass distributions and molecule structures of different chitosans using asymmetrical flow field-flow fractionation combined with multi-angle light scattering. Int. J. Pharm. 351, 23–30.

Barrett, T., Kobayashi, H., Brechbiel, M., Choyke, P.L., 2006. Macromolecular MRI contrast agents for imaging tumor angiogenesis. Eur. J. Radiol. 60, 353–366.

Besheer, A., Hause, G., Kressler, J., Mäder, K., 2007. Hydrophobically modified hydroxyethyl starch: synthesis, characterization, and aqueous self-assembly into nano-sized polymeric micelles and vesicles. Biomacromolecules 8, 359–367.

Besheer, A., Hertel, T.C., Kressler, J., Mäder, K., Pietzsch, M., 2009a. Enzymatically catalyzed HES conjugation using microbial transglutaminase: proof of feasibility. J. Pharm. Sci. 98, 4420–4428.

Besheer, A., Vogel, J., Glanz, D., Kressler, J., Groth, T., Mäder, K., 2009b. Characterization of PLGA nanospheres stabilized with amphiphilic polymers: hydrophobically modified hydroxyethyl starch vs pluronics. Mol. Pharm. 6, 407–415.

Beuf, O., Jaillon, F., Saint-Jalmes, H., 2006. Small-animal MRI: signal-to-noise ratio comparison at 7 and 1.5 T with multiple-animal acquisition strategies. MAGMA 19, 202–208.

Brockmann, M.A., Kemmling, A., Groden, C., 2007. Current issues and perspectives in small rodent magnetic resonance imaging using clinical MRI scanners. Methods 43, 79–87.

Buadu, L.D., Murakami, J., Murayama, S., Hashiguchi, N., Sakai, S., Toyoshima, S., Masuda, K., Kuroki, S., Ohno, S., 1997. Patterns of peripheral enhancement in breast masses: Correlation of findings on contrast medium enhanced MRI with histologic features and tumor angiogenesis. J. Comput. Assist. Tomogr. 21, 421–430.

Caravan, P., 2006. Strategies for increasing the sensitivity of gadolinium based MRI contrast agents. Chem. Soc. Rev. 35, 512–523.

Caravan, P., Ellison, J.J., McMurry, T.J., Lauffer, R.B., 1999. Gadolinium(III) chelates as MRI contrast agents: structure, dynamics, and applications. Chem. Rev. 99, 2293–2352.

Daldrup, H., Shames, D.M., Wendland, M., Okuhata, Y., Link, T.M., Rosenau, W., Lu, Y., Brasch, R.C., 1998. Correlation of dynamic contrast enhanced MR imaging with histologic tumor grade: comparison of macromolecular and small-molecular contrast media. Am. J. Roentgenol. 171, 941–949.

Galiana, G., Branca, R.T., Jenista, E.R., Warren, W.S., 2008. Accurate temperature imaging based on intermolecular coherences in magnetic resonance. Science 322, 421–424.

Gallagher, F.A., Kettunen, M.I., Day, S.E., Hu, D.E., Ardenkjaer-Larsen, J.H., Zandt, R., Jensen, P.R., Karlsson, M., Golman, K., Lerche, M.H., Brindle, K.M., 2008. Magnetic resonance imaging of pH in vivo using hyperpolarized 13C-labelled bicarbonate. Nature 453, 940–943.

Geirnaerdt, M.J.A., Bloem, J.L., Woude, H.-J.F v., Taminiau, d., Nooy, A.H.M., Hogendoorn, M.A.P.C.W., 1998. Chondroblastic osteosarcoma: characterisation by gadolinium-enhanced MR imaging correlated with histopathology. Skeletal Radiol. 27, 145–153.

Geraldes, C.F., Laurent, S., 2009. Classification and basic properties of contrast agents for magnetic resonance imaging. Contrast Media Mol. Imaging 4, 1–23.

Isogai, A., 1997. NMR analysis of cellulose dissolved in aqueous NaOH solutions. Cellulose 4, 99–107.

Kim, J.H., Park, K., Nam, H.Y., Seulki, L., Kim, K., Kwon, I.C., 2007. Polymers for Bioimaging. Prog. Polym. Sci. 32, 1031–1053.
Kobayashi, H., Brechbiel, M.W., 2005. Nano-sized MRI contrast agents with dendrimer cores. Adv. Drug Deliv. Rev. 57, 2271–2286.
Kroft, L.J., Doornbos, J., Benderbous, S., de Roos, A., 1999. Equilibrium phase MR angiography of the aortic arch and abdominal vasculature with the blood pool contrast agent CMD-A2-Gd-DOTA in pigs. J. Magn. Reson. Imaging 9, 777–785.
Kuhl, C.K., 2000. MRI of breast tumors. Eur. Radiol. 10, 46–58.
Kulicke, W.M., Kaiser, U., Schwengers, D., Lemmes, R., 1991. Measurements of the refractive index increment on hydroxyethyl starch as a basis for absolute molecular weight determinations. Starch 43, 392–396.
Kuperman, V., 2000. Magnetic Resonance Imaging – Physical Principles and Applications. Academic Press, New York.
Lauterbur, P.C., 1973. Image formation by induced local interactions: examples employing nuclear magnetic resonance. Nature 242, 190–191.
Lide, D.R., 2004. CRC Handbook of Chemistry and Physics, 85th ed. CRC Press, Boca Raton, FL.
Logothetis, N.K., 2008. What we can do and what we cannot do with fMRI. Nature 453, 869–878.
Loubeyre, P., Canet, E., Zhao, S., Benderbous, S., Amiel, M., Revel, D., 1996. Carboxymethyl-dextran-gadolinium-DTPA as a blood-pool contrast agent for magnetic resonance angiography. Experimental study in rabbits. Invest. Radiol. 31, 288–293.
Ma, L.D., Frassica, F.J., McCarthy, E.F., Bluemke, D.A., Zerhouni, E.A., 1997. Benign and malignant musculoskeletal masses: MR imaging differentiation with rim-to-center differential enhancement ratios. Radiology 202, 739–744.
Metz, H., Mäder, K., 2008. Benchtop-NMR and MRI – a new analytical tool in drug delivery research. Int. J. Pharm. 364, 170–175.
Mitchell, D.G., Saini, S., Weinreb, J., Lange, E.E.D., Runge, V.M., Kuhlman, J.E., Parisky, Y., Johnson, C.D., Brown, J.J., Schnall, M., Herfkens, R.J., Davis, P.L., Gorczyca, D., Sica, G., Foster, G.S., Bernardino, M.E., 1994. Hepatic metastases and cavernous hemangiomas: distinction with standard- and triple-dose gadoteridol-enhanced MR imaging. Radiology 193, 49–57.
Morris, E.A., 2002. Breast cancer imaging with MRI. Radiol. Clin. North Am. 40, 443–466.
Mulder, W.J.M., Strijkers, G.J., Tilborg, G.A.F., Griffioen, A.W., Nicolay, K., 2006. Lipid-based nanoparticles for contrast-enhanced MRI and molecular imaging. NMR Biomed. 19, 142–164.
Mussurakis, S., Gibbs, P., Horsman, A., 1998. Peripheral enhancement and spatial contrast uptake heterogeneity of primary breast tumours: quantitative assessment with dynamic MRI. J. Comput. Assist. Tomogr. 22, 35–46.
Ogan, M.D., Schmiedl, U., Moseley, M.E., Grodd, W., Paajanen, H., Brasch, R.C., 1987. An intravascular contrast-enhancing agent for magnetic resonance blood pool imaging: preparation and characterization. Invest. Radiol. 22, 665–671.
Rebizak, R., Schaefer, M., Dellacherie, E., 1997. Polymeric conjugates of Gd3+-diethylenetriaminepentaacetic acid and dextran. 1. Synthesis characterization, and paramagnetic properties. Bioconj. Chem. 8, 605–610.
Roger, P., Bauda, B., Colonna, P., 2001. Characterization of starch polysaccharides by flow field-flow fractionation-multi-angle laser light scattering-differential refractometer index. J. Chromatogr. A 917, 179–185.
Rolland-Sabate, A., Colonna, P., Mendez-Montealvo, M.G., Planchot, V., 2007. Branching features of amylopectins and glycogen determined by asymmetrical flow field flow fractionation coupled with multiangle laser light scattering. Biomacromolecules 8, 2520–2532.
Schwickert, H.C., Roberts, T.P.L., Mühler, A., Stiskal, M., Demsar, F., Brasch, R.C., 1995. Angiographic properties of Gd-DTPA-24-cascade-polymer – a new macromolecular MR contrast agent. Eur. J. Radiol. 20, 144–150.
Tsien, C., Gomez-Hassan, D., Haken, R.K.T., Tatro, D., Junck, L., Chenevert, T.L., Lawrence, T., 2005. Evaluating changes in tumor volume using magnetic resonance imaging during the course of radiotherapy treatment of high-grade gliomas: implications for conformal dose-escalation studies. Int. J. Radiat. Oncol. Biol. Phys. 62, 328–332.
Varallyay, C.G., Muldoon, L.L., Gahramanov, S., Wu, Y.J., Goodman, J.A., Li, X., Pike, M.M., Neuwelt, E.A., 2009. Dynamic MRI using iron oxide nanoparticles to assess early vascular effects of antiangiogenic versus corticosteroid treatment in a glioma model. J. Cereb. Blood Flow Metab. 29, 853–860.
Wittgren, B., Wahlund, K.G., Andersson, M., Arfvidsson, C., 2002. Polysaccharide characterization by flow field-flow fractionation-multiangle light scattering: Initial studies of modified starches. Int. J. Polym. Anal. Character. 7, 19–40.